
This is an electronic reprint of the original article.
This reprint may differ from the original in pagination and typographic detail.

Ghahfarokhi, Payam Shams; Kallaste, Ants; Belahcen, Anouar; Vaimann, Toomas; Rassõlkin, Anton

Hybrid thermal model of a synchronous reluctance machine

Published in:
Case Studies in Thermal Engineering

DOI:
[10.1016/j.csite.2018.05.007](https://doi.org/10.1016/j.csite.2018.05.007)

Published: 01/09/2018

Document Version
Publisher's PDF, also known as Version of record

Published under the following license:
CC BY-NC-ND

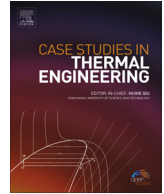
Please cite the original version:
Ghahfarokhi, P. S., Kallaste, A., Belahcen, A., Vaimann, T., & Rassõlkin, A. (2018). Hybrid thermal model of a synchronous reluctance machine. *Case Studies in Thermal Engineering*, 12, 381-389.
<https://doi.org/10.1016/j.csite.2018.05.007>

This material is protected by copyright and other intellectual property rights, and duplication or sale of all or part of any of the repository collections is not permitted, except that material may be duplicated by you for your research use or educational purposes in electronic or print form. You must obtain permission for any other use. Electronic or print copies may not be offered, whether for sale or otherwise to anyone who is not an authorised user.



Contents lists available at ScienceDirect

Case Studies in Thermal Engineering

journal homepage: www.elsevier.com/locate/csite

Hybrid thermal model of a synchronous reluctance machine

Payam Shams Ghahfarokhi^{a,*}, Ants Kallaste^a, Anouar Belahcen^b, Toomas Vaimann^a, Anton Rassõlkin^a^a Electrical Power Engineering and Mechatronics, Tallinn University of Technology, Ehitajate tee 5, Tallinn, Estonia^b Electrical Engineering and Automation, Aalto University, Espoo, Finland

A B S T R A C T

This paper presents a hybrid thermal modeling methodology to analyze the temperature performance of radial flux electrical machines. For this purpose, the 2D finite element model of the active part of the machine is coupled with a lumped parameters thermal circuit of the end-winding region. A synchronous reluctance machine is used to validate the proposed approach. The results from the proposed method are compared with the experimental ones, which are obtained from a prototype machine. The computations show that the 2D FE model underestimates the temperature rise in the machine as it does not account for the power losses in the end-windings. The hybrid model accounts for these losses as well as for the heat dissipation in the end-winding region.

1. Introduction

According to the efforts to achieve higher torque and power density, higher energy efficiency and cost reduction in the design of new generation of electrical machines, the thermal design of electrical machine in parallel with the electromagnetic design has acquired a particular importance [1].

The thermal analysis of an electrical machine is divided into two groups; the lump parameters thermal network (LPTN) and the finite element analysis (FEA) [1,2]. The LPTN is a common method for thermal analysis of key components of the electrical machine. There are many reports from the literature on the thermal analysis of different electrical machines, e.g., [3–7]. The main advantage of this method over the FEA is the short calculation time with acceptable accuracy [2,8]. The FEA needs high setup and computational time, but it is considered to be more accurate in modeling the loss distribution and thus the temperature rise in the machines [2,8,9].

An electrical machine can be modeled with the FEA in a 2D or 3D approach [9]. Modeling the electrical machine by the 3D FEA is a very time-consuming process and consist of several complex geometry setups e.g., end-windings. Accordingly, in order to reduce the computation time and use the benefits of FEA for monitoring the thermal behavior of the electrical machine, the 2D FEA is usually implemented. There are many reports on the thermal modeling of electrical machines by 2D FEA [9–14], among others. However, there are some problems in the 2D FEA thermal models of electrical machines. As an example, in [10], the author neglected the axial heat flow from the end-winding to the active part of the machine and in [11], the paper presents a 2D FEA where the results are compared with a simplified LPTN which is not including the end-winding thermal effect. Since they applied the simplified assumption to neglect the heat transfer from the end-windings to the slots, they could not model the hottest spot of the electrical machine and the whole temperature distribution is underestimated. As a result, these models cannot provide a correct view of the heat transfer and thermal analysis for an electrical machine. In order to remedy this simplification, as well as using the advantages of the 2D FEA, we

* Corresponding author.

E-mail address: payam.shams@ttu.ee (P.S. Ghahfarokhi).

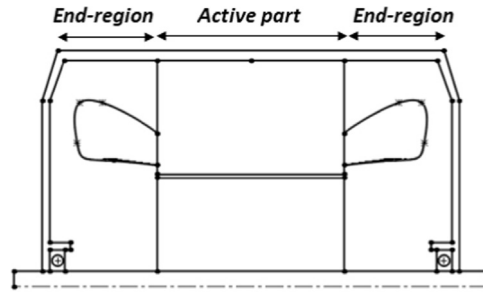


Fig. 1. The axial cross-section of the electrical machine.

propose a hybrid thermal model, which consist of coupling 2D FEA with the equivalent thermal circuit. Such an approach is very common in the electromagnetic analysis of electrical machines, where the end-winding impedance is added in the winding circuit equations and coupled with the 2D field equations.

The coupling methodology can be divided into two types; direct and indirect coupling. The direct coupling method requires access to the 2D system matrix assembly routine to add the circuit terms and solve all the equations simultaneously. Such an approach although fast is not possible to implement in a general purpose software unless one has access to the code. In this paper, we choose the indirect approach as explained in the methods section. We focus on the application of this method in the steady-state thermal analysis of a synchronous reluctance motor (SynRM). The temperature of the active part of the machine is modeled by means of a 2D FEA simulation software and the temperature effect of the end-winding region of the machine is evaluated by an equivalent thermal circuit. The two models are combined through an iterative procedure.

2. The hybrid thermal model details

Fig. 1 shows an illustration of the axial cross section of an electrical machine. According to this figure, the construction of the electrical machine is divided into two main sections, the magnetic active part of the machine and the end-winding region. The 2D FEA can model only the heat transfer within the active part of the machine. It does not take into account the effect of heat transfer between the end-winding region and these active parts. One possibility to tackle this issue is to include the power losses in the end-winding in the slot losses while compiling the 2D model of the machine. However, this would result in an overestimation of the temperatures, as a large part of the end-winding losses is flowing through the end-winding region and not transferred to the active parts. Yet a better approach is the proposed hybrid model. The hybrid thermal model is constructed by coupling the 2D FEA model of the active parts and the lumped parameters thermal network model of the end-winding region.

The hybrid thermal model described above is applied to a four poles 11 kW, 400 V, 50 Hz, transverse-laminated radial flux SynRM with F insulation class. Fig. 2 shows a CAD drawing of the machine and its cross section. Tables 1 and 2 give the geometrical and material data of the prototype SynRM.

2.1. The FEA thermal model

As mentioned, in the hybrid thermal calculation method, the active parts of the machine are modeled by using a 2D FEA software. In order to model the heat transfer of the active part of the machine, the FEMM package software is selected. This software has some advantages, e.g., free license software with a Matlab toolbox called OctaveFEMM to provide a way for operating the FEMM solver via Matlab functions [15].

The main challenges with the FEA are how to define the thermal conductivity of the composite materials inside the slots such as the copper conductors, the conductor insulation, the impregnation material and the slot insulation [1]; and how to implement the convection and radiation phenomena.

The slot area consists of different materials with different thermal conductivities. Due to the small dimensions of the materials layer in the slot, it is not practical to model each material separately. To solve this problem, an equivalent thermal conductivity k_e of the slot area is defined as in [16]:

$$k_e = k_2 \frac{(1 + f_1)k_1 + (1 - f_1)k_2}{(1 - f_1)k_1 + (1 + f_1)k_2}, \quad (1)$$

where k_1 is the thermal conductivity of the copper conductors, k_2 is the thermal conductivity of the slot impregnation, f_1 is the volume fraction of the conductor in the slot and f_2 is the volume fraction of the impregnation in the slot (with $f_1 + f_2 = 1$). The other insulation materials are assumed equivalent to the impregnation material, which is a well-justified assumption as explained in [16].

The heat is transferred from the exterior surface of the electrical machine to the ambient by the convection and radiation phenomena. These phenomena are implemented into the 2D FE model by defining the boundary condition on the outer surface of the model to describe the quality of the heat transfer from the outer surface of the machine to the ambient. In an actual machine, the outer surface consists of axial cooling fins, which can be modeled in the FEA analysis but this will result in a very dense mesh and thus

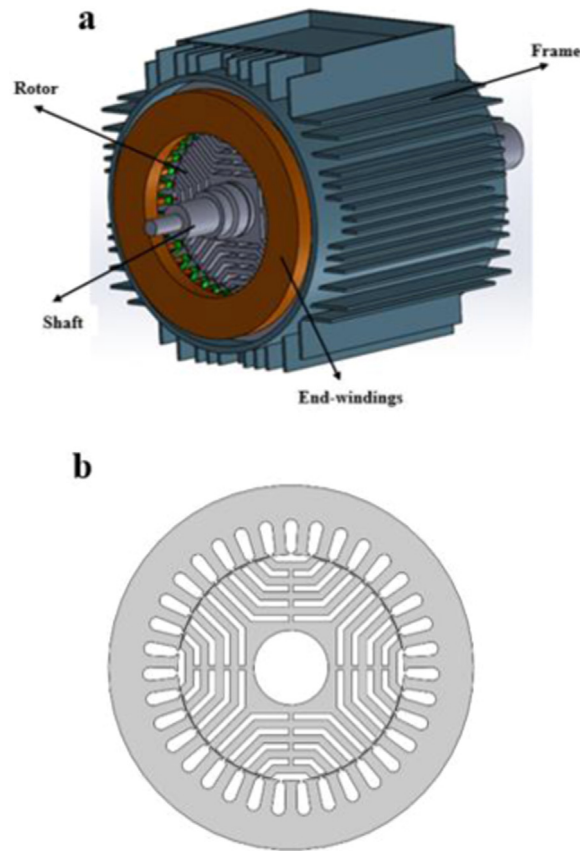


Fig. 2. Structure and Topology of transverse-laminated SynRM analyzed in this paper.

Table 1
Geometrical data of the transverse- laminated SynRM.

Name	Symbol	Unit	Value
Stator core length	L_s	mm	156
Stator inner diameter	D_{is}	mm	136
Stator outer diameter	D_{os}	mm	219
Number of slots	N_s	–	36
Air-gap height	h_{ag}	mm	0.4
Rotor inner diameter	D_{ir}	mm	45
Rotor outer diameter	D_{or}	mm	135.2
Slot height	h_1	mm	21
Slot filling factor	k_f	–	0.6
Slot area	S_s	mm ²	130.1

Table 2
Material data of transverse- laminated SynRM.

Machine part	Material	Thermal conductivity symbols	Thermal conductivity (W/mK)
Frame	Aluminum	k_{al}	230
Laminations	Electric steel	k_{ir}	28
Winding	Copper	k_{cu}	387
Impregnation	Resin	k_2	0.2
Air gap	Air	k_{air}	0.0257
Shaft	Steel	k_{sh}	41

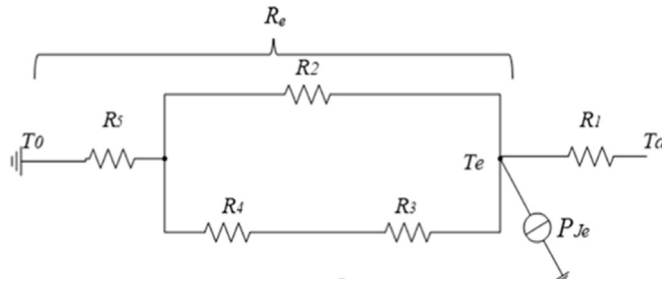


Fig. 3. The equivalent thermal circuit of the end-windings.

very slow computations. In order to reduce the model size, a modified smooth outer surface is used and the effect of the cooling fins is accounted for through an equivalent heat transfer coefficient h' , which is calculated as in [14]:

$$h' = \frac{s}{s'}h, \tag{2}$$

where h is the actual heat coefficient, $s = 0.4 \text{ m}^2$ is the actual outer surface of the active part of the machine including the fins and $s' = 0.11 \text{ m}^2$ is the simplified outer surface.

2.2. Lumped parameters thermal network

Since the 2D FEA does not take into account the effect of heat transfer through the end-winding region of the electrical machine a lumped parameters thermal network of these parts of the machine is developed and coupled with the FEA.

The developed lumped parameters thermal network is valid for the steady-state operation. It consists of thermal resistances and power sources as shown in Fig. 3. The main assumption for this construction is the fact that the power losses distribution is assumed uniform in the end-windings, which are represented as a toroidal structure. Yet another assumption is that the heat flux distribution in both end regions of the machine are analogous. This later assumption could be removed if one makes separate thermal models for each end-winding.

The variables in the LPTN of Fig. 3 are T_a and T_e , which represent the average temperatures of the slots and the end-windings respectively. The model consists of two nodes and five thermal resistances as well as the end winding copper losses as a heat source. Table 3 describes the definition of the thermal model components of Fig. 3.

The value of the thermal resistances of Table 3 are computed with an acceptable accuracy by the following analytical equations:

$$R_1 = \frac{l_{av}}{6N_s k_{cu} s_{cu}}, \tag{3}$$

$$l_a = L_s + 1.2\tau_p + l', \tag{4}$$

where $l_{av} = 0.321 \text{ m}$ is the average conductor length of half a turn, N_s is the number of the stator slots, k_{cu} is the thermal conductivity of the copper, $s_{cu} = 7.8 \times 10^{-5} \text{ m}$ is the total copper conductor cross-section area, $\tau_p = 0.096 \text{ m}$ is the pole pitch, and $l' = 0.05 \text{ m}$ is an empirically determined constant, depending on the size of the machine [4].

$$R_2 = \frac{1}{2\pi k_{air} (L_f - L_s)} \ln\left(\frac{r_{oy}}{r_{oy} - 0.5t_{sy}}\right), \tag{5}$$

where $L_f = 0.222 \text{ m}$ is the frame length, L_s is the stator core length, r_{oy} is the outer stator yoke radius, t_{sy} is the stator radius height and k_{air} is the air conductivity [8].

$$R_3 = \frac{1}{s_{ew} h_{ew}}, \tag{6}$$

where $s_{ew} = 0.03 \text{ m}^2$ is the total surface of the end-windings in contact with the inner air and $h_{ew} = 15.5 \text{ W}/(\text{m}^2\text{K})$ is the convection

Table 3
Definition and the values of the thermal model components.

Component	Value	Unit	Description
R_1	0.05	K/W	Conduction thermal resistance between the midpoint of end-winding and the midpoint of coil side
R_2	10.7	K/W	Conduction thermal resistance between the stator winding and the frame
R_3	2.3	K/W	Convection thermal resistances between the stator end-winding and inner air of the end region
R_4	0.8	K/W	Convection thermal resistance between the inner air and the end cap
R_5	0.6	K/W	Total heat extraction thermal resistance from the frame to the ambient
P_{Je}	98.3	W	Stator end-winding Joule losses

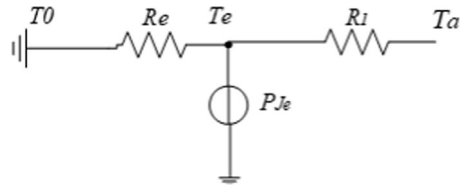


Fig. 4. The final equivalent thermal circuit after lumping R_2 to R_5 into R_e .

coefficient for the air between the end-windings and the inner air, which are calculated as follow [4,8]:

$$s_{ew} = (L_f - L_s)2\pi r_{is}, \tag{7}$$

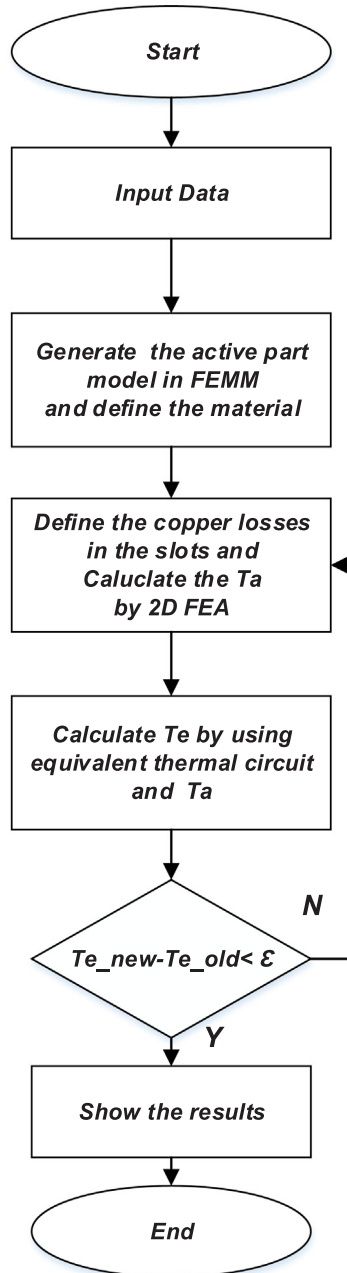


Fig. 5. The flow chart of hybrid model calculation.

$$h_{ew} = 15.5(0.29\nu+1) \tag{8}$$

$$\nu = r_{or} \omega \eta, \tag{9}$$

where r_{is} is the inner stator radius, ν is the inner air speed, r_{or} is the outer rotor radius; ω is the rotor angular speed and η is the fan efficiency and according to [3] it is equal to 0.5.

$$R_4 = \frac{1}{s_{ec} h_{ec}}, \tag{10}$$

where $s_{ec} = 0.08 \text{ m}^2$ is the external surface of the two machine end-caps and h_{ec} is the convection coefficient between the inner air gap and the end-cap, which is equal to the value of h_{ew} [4].

$$R_5 = \frac{1}{s_e h_e}, \tag{11}$$

where $s_e = 0.22 \text{ m}^2$ is the lateral outer surface of the SynRM and $h_e = 7.1 \text{ W}/(\text{m}^2\text{K})$ is the total heat extraction coefficient from the outer surface, which consists of the sum of the radiation and convection coefficients.

2.3. Hybrid model calculation

The LPNT of Fig. 3 is further simplified by combining the thermal resistances R_2 to R_5 in a single equivalent resistance R_e as:

$$R_e = \frac{(R_4 + R_3) \times R_2}{R_2 + R_3 + R_4} + R_5. \tag{12}$$

Fig. 4 shows the final LPNT used in the hybrid thermal model.

The end-windings and slot copper loss are evaluated from the total copper loss based on the volumes of the copper conductors in the slots and in the end-windings. The temperature of the end-windings T_e , and the amount of heat transfer from the end-windings to slots P_{ex} , are evaluated by applying the Kirchhoff current rule as follow:

$$T_e = \left(P_{je} + \frac{T_0}{R_e} + \frac{T_a}{R_1} \right) (R_1 + R_e), \tag{13}$$

$$P_{ex} = \frac{T_e - T_a}{R_1}. \tag{14}$$

where the temperature of the active parts T_a is evaluated by the FEA and P_{ex} is the amount of losses added to the slot losses in the FEA at each iteration. Note that P_{ex} can be negative in some cases.

Fig. 5 shows the flowchart of the hybrid model calculation. After the construction of the FE model and the definition of the materials, the copper power losses are inserted in the model. In the first iteration step, the FEA calculates the temperature of the active part of the machine and predicts the average value of the slot temperature T_a . T_e and P_{ex} are then calculated by (13) and (14) respectively. In the next iteration, P_{ex} is added to the active copper losses in the FE model. This iteration process will continue until the difference between the previous T_e and the new one is smaller than an arbitrary defined accuracy \mathcal{E} , which was 0.01 K in our case.

The FE model requires some parameters, such as the losses and the radiation and convection heat transfer coefficients at the outer surface. These parameters have been evaluated experimentally as explained in the following section.

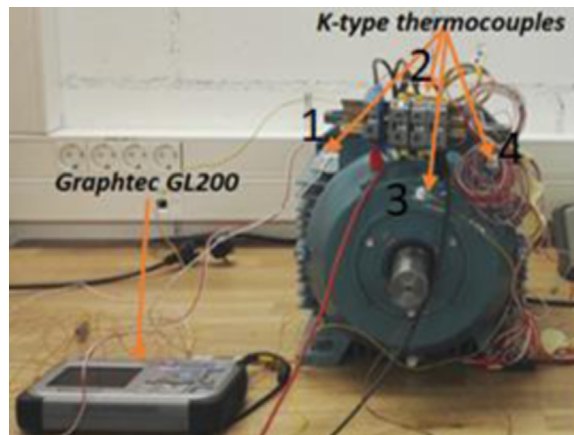


Fig. 6. Test setup.

3. Experimental methodology

The objective of the experimental work is to determine the heat extraction coefficient and the copper losses. The accuracy of the calculation based on the hybrid model is also evaluated by comparing the computation and measurement results.

The total heat extraction coefficient for the natural cooling is evaluated by using the DC stator test. In this test, the losses of the machine are confined to the Joule loss of the stator windings where the electric power can be easily measured. In the calculations, we accounted for the variations in the winding electrical resistance, as the winding resistivity is temperature dependent [7,17]. During the experiments, the DC power applied to the motor is measured as well as the surface temperature of the motor at different locations. Four K-type thermocouples are installed by means of adhesive material in various locations on the frame surface of the motor. The ambient temperature is also measured by means of a K-type thermocouple. For the purpose of increasing the accuracy of the temperature measurement and minimizing the contact resistance between the thermocouples and the frame surface of the motor, we used thermal paste. The average temperature of these four thermocouples is assumed to be the mean temperature of the motor frame surface. During the experiments, all the temperature data are collected by means of a Graphtec GL200 logger. The experiment has been carried in the thermal steady-state condition. The total heat extraction coefficient h_e is calculated as [18]:

$$h_e = \frac{P}{(T_s - T_0)S}, \tag{15}$$

where T_s is the frame surface temperature, T_0 is the ambient temperature, $S = 0.69 \text{ m}^2$ is the total surface area of the frame and P is the input electric DC power.

Fig. 6 shows the experimental setup and the different location of the surface frame K type thermocouples. In addition to the surface temperature, the temperature inside the machine was also measured. For this purpose, six different RTD PT100 have been installed inside the end-windings and slots of the stator. These measured temperatures are used to validate the hybrid thermal model results.

3.1. Uncertainty analysis of experimental results

In this sub section, we determined the total accuracy of experimental data according to the accuracy of the measurement instruments. During the experiment, the voltage and current are measured with the TTI QPX1200S. The accuracy of the voltage and current readings are 0.1% and 0.3% respectively. Furthermore, the standard accuracy of the K-type thermocouple is 0.75%. According to [19], the power uncertainty is evaluated as:

$$\omega_{Q_T} = \left[\left(\frac{\partial Q_T}{\partial V} \cdot \omega_V \right)^2 + \left(\frac{\partial Q_T}{\partial I} \cdot \omega_I \right)^2 \right]^{0.5}, \tag{16}$$

where ω_{Q_T} , ω_V and ω_I are the uncertainties in the total input power, voltage and current.

This leads to the uncertainty for the computed convection coefficient as:

$$\omega_h = \left[\left(\frac{\partial h}{\partial Q_T} \cdot \omega_{Q_T} \right)^2 + 2 \cdot \left(\frac{\partial h}{\partial T} \cdot \omega_T \right)^2 \right]^{0.5}, \tag{17}$$

where ω_T is the uncertainty in the temperature measurement.

It should be noted that the maximum uncertainty in the computed convection coefficients is 6.2%.

4. Results and discussion

The hybrid model is applied for the same operating condition as in the experiment, i.e. DC test. The comparison is carried out for the hybrid model, the experimental results, and a simple 2D model that does not account for the end-windings.

As Fig. 6 shows, each sensor is marked with a number. Accordingly, Table 4 shows the measured temperature by the thermocouples which have been install on the outer surface of the SynRM.

The experimental test resulted in a frame surface mean temperature of 61.2 °C for a DC input power of 191.1 W, while the ambient temperature was 21.8 °C. The standard deviation of the frame temperature as calculated from the four sensors was ± 2.2 °C. Fig. 7 shows the temperature distribution around the frame surface. From these values, the total heat extraction coefficient calculated by (15) is 7.1 W/Km². The equivalent thermal conductivity of the slot and its modified total heat extraction coefficient, calculated by (1) and (2) respectively, are 0.79 W/(Km) and 27 W/(Km²). The evaluated copper losses produced in the slots and end-windings are 92.8 W and 98.3 W respectively. These values were used in the FE part of the hybrid model.

Table 4
surface temperature of the SynRM.

	1 (°C)	2 (°C)	3 (°C)	4 (°C)
Surface temperature of the SynRM	61.7	64.4	58.7	60.3

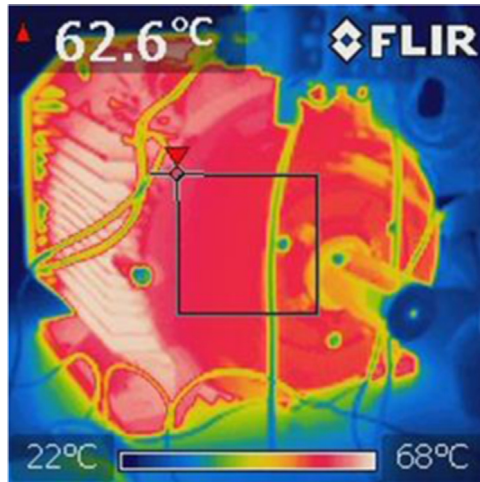


Fig. 7. Temperature distribution over the frame surface.

Table 5

Measured and calculated temperatures.

	Hybrid Model (°C)	2D FEA (°C)	Experimental (°C)
Slot	72.9	51.9	74 ± 2.2
End-winding	78.5	–	78 ± 0.15

Table 5 shows the steady-state temperature results of the end-windings and slots from the three methods;

According to Table 5, there is a significant difference in the predicted temperature between the hybrid thermal model and the simple 2D FE model, around 21 °C. Furthermore, the hybrid thermal model results are in a good agreement with the experimental ones. This proves that the proposed method can be implemented to predict the temperatures of the machine with a high accuracy.

Figs. 8 and 9 show the temperature distribution in the active part of the machine computed with the hybrid thermal model and 2D FEA respectively. The hottest parts of the machine's active part are the slots as would be expected. The two distributions look alike, except that the results from the hybrid model are around 21 °C higher than for the FE Model. This is due to the fact that part of the end-winding heat is flowing to the slots.

The results of this study indicate that the 2D FEA cannot be used alone for heat transfer modeling unless additional considerations are given to the end-windings and possibly to the shaft. The computations with the hybrid model show that a considerable amount of heat (61.98% of the end-windings losses) is transferred from the end-windings to the slots.

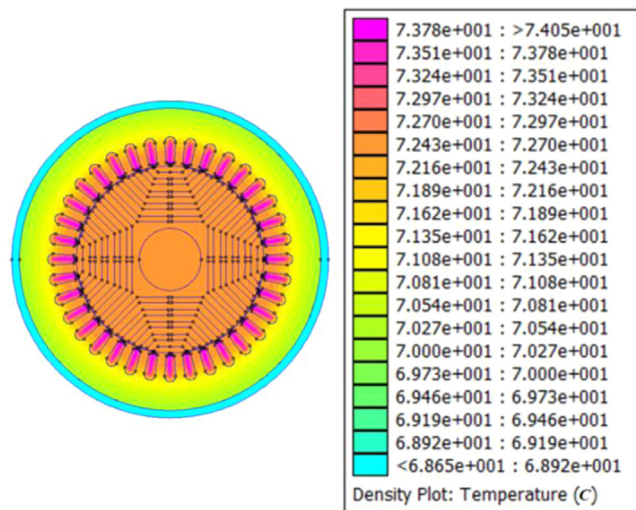


Fig. 8. Temperature distribution in the active part of the machine by using the hybrid model.

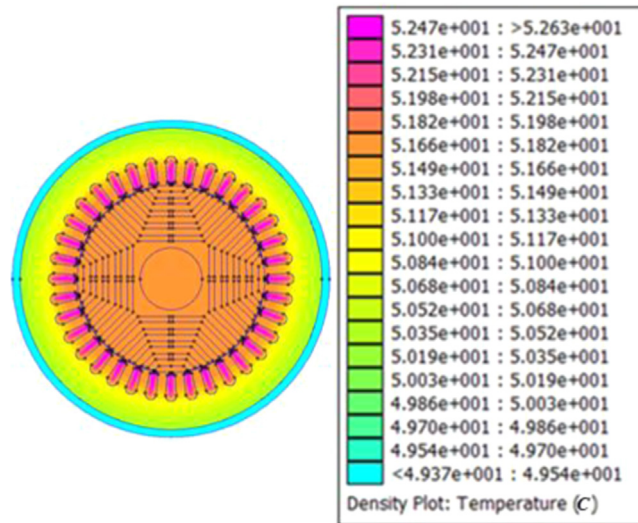


Fig. 9. Temperature distribution in the active part of the machine by using the only 2D FEA and simplifying assumption.

5. Conclusion

The focus of this paper has been to develop a hybrid thermal model, which consists of a 2D FE model for the active part of the machine and a Lumped Parameters Thermal Network for the end-region section. This model makes it possible to predict the temperature rise of the different sections of the electrical machine e.g., end-windings, slots, rotor, stator teeth, and yoke, with a higher accuracy than the simple 2D FE model alone. This hybrid model is a good alternative to the 3D FE models, which require high and unaffordable computation time. The accuracy of the model is still good as the results of the model are in good agreement with the experimental setup.

Acknowledgments

This research has been supported by the Estonian Research Council under grant PUT1260.

References

- [1] P.S. Ghahfarokhi, A. Kallaste, A. Belahcen, T. Vaimann, A. Rassolkin, Review of thermal analysis of permanent magnet assisted synchronous reluctance machines, *Electr. Power Qual. Supply Reliab.* (2016) 219–224.
- [2] A. Boglietti, A. Cavagnino, D. Staton, M. Shanel, M. Mueller, C. Mejuto, Evolution and modern approaches for thermal analysis of electrical machines, *IEEE Trans. Ind. Electron.* 56 (3) (2009) 871–882.
- [3] P.H. Mellor, D. Roberts, D.R. Turner, Lumped parameter thermal model for electrical machines of TEFC design, *IEE Proc. B Electr. Power Appl.* 138 (5) (1991) 205.
- [4] A. Boglietti, A. Cavagnino, M. Lazzari, M. Pastorelli, A simplified thermal model for variable-speed self-cooled industrial induction motor, *IEEE Trans. Ind. Appl.* 39 (4) (2003) 945–952.
- [5] J. Lindström, Thermal Model of a Permanent-Magnet Motor for a Hybrid Electric Vehicle, Chalmers university of technology, Goteborg, 1999.
- [6] A.M. EL-Refaie, N.C. Harris, T.M. Jahns, K.M. Rahman, Thermal analysis of multibarrier interior PM synchronous machine using lumped parameter model, *IEEE Trans. Energy Convers.* 19 (2) (2004) 303–309.
- [7] P.S. Ghahfarokhi, A. Kallaste, A. Belahcen, T. Vaimann, Steady state and transient thermal analysis of the stator coil of a permanent magnet generator, in: *Proceedings of the 18th International Scientific Conference on Electric Power Engineering (EPE)*, 2017, pp. 1–5.
- [8] A. Boglietti, A. Cavagnino, D. Staton, Determination of critical parameters in electrical machine thermal models, *IEEE Trans. Ind. Appl.* 44 (4) (2008) 1150–1159.
- [9] V. Matošević, Ž. Štih, 2D Magneto-thermal analysis of synchronous generator, *Przegład Elektrotech.* 2014 (2016) 157–160.
- [10] Weili Li Junci Cao Fei Huo Jiafeng Shen, Numerical analysis of stator-rotor coupled transient thermal field in induction motors with blocked rotor. in: *Proceedings of the Automation Congress, 2008, WAC 2008 World*: date, Sept. 28 2008–Oct. 2 2008. 2008 pp.1–6.
- [11] R.-J. Wang, G.C. Heyns, Thermal analysis of a water-cooled interior permanent magnet traction machine, in: *Proceedings of the IEEE International Conference on Industrial Technology (ICIT)*, 2013, pp. 416–421.
- [12] J. Driesen, R. Belmans, K. Hameyer, A. Arkkio, T. Jokinen, Efficient magnetic-thermal coupled simulation of electrical machines using a double combined FEM-circuit approach, in: *Proceedings of the International Conference on Electrical machines, ICEM'98, Istanbul, Turkey, 2–4 September 1998*, 1998, pp. 1402–1407.
- [13] S. LIPiŃSKI, K. Grunt, J. Zawilak, 2D steady-state thermal analysis of a line-start, permanent magnet synchronous motor, *PRZEGLĄD Elektrotech.* 1 (3) (2017) 183–186.
- [14] V. Hatziaathanassiou, J. Xypteras, G. Archontoulakis, Electrical-thermal coupled calculation of an asynchronous machine, *Arch. für Elektro.* 77 (2) (1994) 117–122.
- [15] Finite Element Method Magnetics: OctaveFEMM. [Online]. Available: <<http://www.femm.info/wiki/octavefemm>>.
- [16] M. Popescu, D. Staton, D. Dorrell, F. Marignetti, and D. Hawkins, “Study of the thermal aspects in brushless permanent magnet machines performance,” in: *Proceedings of the IEEE Workshop on Electrical Machines Design, Control and Diagnosis (WEMDCD)*, 2013, pp. 60–69.
- [17] A.R. PayamShams, Ghahfarokhi, Ants Kallaste, Anouar Belahcen, Toomas Vaimann, Determination of Forced Convection Coefficient Over a Flat Side of Coil, in: *Proceedings of the 58th International Scientific Conference on Power and Electrical Engineering of Riga Technical University (RTUCON)*, 2017, pp. 1–4.
- [18] P. shams Ghahfarokhi, A. Kallaste, and A. Belahcen, Determination of thermal convection coefficient from coil's flat plate side. in: *Proceedings of the 16th International Symposium Topical Problems in the Field of Electrical and Power Engineering and Doctoral School of Energy and Geotechnology III*. 2017, pp. 130–132.
- [19] M. Ahmadi, G. Mostafavi, M. Bahrami, Natural convection from rectangular interrupted fins, *Int. J. Therm. Sci.* 82 (2014) 62–71.